



# Optics Letters

## Surface-enhanced Raman scattering of monolayer transition metal dichalcogenides on Ag nanorod arrays

LIQIN SU,<sup>1,2</sup> LAYNE BRADLEY,<sup>3</sup> YILING YU,<sup>4</sup> YIFEI YU,<sup>4</sup> LINYOU CAO,<sup>4</sup> YIPING ZHAO,<sup>3</sup> AND YONG ZHANG<sup>2,\*</sup>

<sup>1</sup>College of Optical and Electronic Technology, China Jiliang University, Hangzhou, 310018, China

<sup>2</sup>Department of Electrical and Computer Engineering, The University of North Carolina at Charlotte, Charlotte, North Carolina 28223, USA

<sup>3</sup>Department of Physics and Astronomy, Nanoscale Science and Engineering Center, The University of Georgia, Athens, Georgia 30602, USA

<sup>4</sup>Department of Materials Science and Engineering, North Carolina State University, Raleigh, North Carolina 27695, USA

\*Corresponding author: yong.zhang@uncc.edu

Received 29 July 2019; revised 11 October 2019; accepted 15 October 2019; posted 18 October 2019 (Doc. ID 373880); published 8 November 2019

**In this work, we studied surface-enhanced Raman scattering (SERS) of  $MS_2$  ( $M = Mo, W$ ) monolayers that were transferred onto Ag nanorod arrays. Compared to the suspended monolayers, the Raman intensity of monolayers on an Ag nanorod substrate was strongly enhanced for both in-plane and out-of-plane vibration modes: up to 8 (5) for  $E_{2g}$  and 20 (23) for  $A_{1g}$  in  $MoS_2$  ( $WS_2$ ). This finding reveals a promising SERS substrate for achieving uniform and strong enhancement for two-dimensional materials in the applications of optical detecting and sensing.** © 2019 Optical Society of America

<https://doi.org/10.1364/OL.44.005493>

In the family of two-dimensional (2D) transition metal dichalcogenides (2D-TMDs), monolayer  $MS_2$  ( $M = Mo, W$ ) have been shown to exhibit many interesting electronic and optical properties. As an active material, the ultra-thin nature of the 2D layer makes its interaction with light relatively weak on its own, which results in inefficient light absorption and emission, and weak Raman scattering. Moderate enhancement of the interaction has been demonstrated when they are grown on or transferred onto various dielectric substrates [1–3]. However, adding metallic, typically Au or Ag, nanostructures on the 2D layer can potentially yield more significant enhancement and/or modification of the interaction through a plasmonic effect, which has resulted in a great boost of light absorption [4–6], photoluminescence (PL) [7], and modification in Raman scattering [7,8] of the 2D layer. More sophisticated enhancement schemes have also been explored [9]. Nanometallic-particle decorated 2D layers are also interesting in optical sensing applications because the metallic particles can serve as hot spots for surface-enhanced Raman scattering (SERS) of molecules deposited on the 2D layer [7,10–15]. We note that the reported plasmonic enhancement has typically achieved by depositing the metallic nanostructures on the upper surface of the 2D layer, which is not a convenient structure for further device processing, and

the enhancement is spatially selective thus nonuniform [16,17]. For many practical applications, it would be more desirable that the plasmonic structure is below the 2D layer and can offer a spatially uniform enhancement, i.e., with a high density of regularly distributed hot spots [18].

In this work, we investigate plasmonic enhancement effect on Raman scattering in  $MS_2$  monolayers that were originally grown by chemical vapor deposition (CVD) and then transferred onto a thin layer of high density, quasi-regularly distributed Ag nanorods (AgNRs). Approximate enhancement factors of two to twenty-three, depending on vibrational modes and materials, have been observed compared to the suspended film. This finding can potentially enable using large-scale CVD-grown 2D-TMD monolayers for various optoelectronic and sensing applications.

The AgNRs were formed by a physical vapor deposition technique known as oblique angle deposition (OAD) on glass slides with fabrication and structure characterization details described in previous publications [19,20]. The average nanorod length is  $\sim 1000$  nm as measured by a calibrated quartz crystal microbalance monitor. The AgNRs are typically inclined at an oblique angle  $\theta$  from the substrate normal. This angle is tunable by changing the substrate tilt. The ones used in this study have  $\theta$  of  $\sim 70^\circ$ . Figures 1(a) and 1(b) show representative top-view and tilted-view SEM images of the AgNR substrate. The diameter of the nanorods is approximately 100–150 nm. The AgNR array substrate has been shown to offer uniform and high SERS enhancement for probing dye molecules with the maximum enhancement factor  $\sim 5 \times 10^8$  [19,20]. The high quality monolayer  $MS_2$  films were grown on sapphire substrate by using a CVD process on sapphire substrates with details reported before [21].

Transferring a  $MS_2$  film onto a AgNR substrate was carried out by a method that we developed previously [22]. With the assistance of polystyrene (PS) and a water droplet, the  $MS_2$  film was peeled off the sapphire substrate, and then transferred onto the AgNR substrate. After the transfer process, the samples were baked at  $150^\circ\text{C}$  for 5 min to further remove the PS and other polymer residues. Figures 1(c)–1(d) show the optical

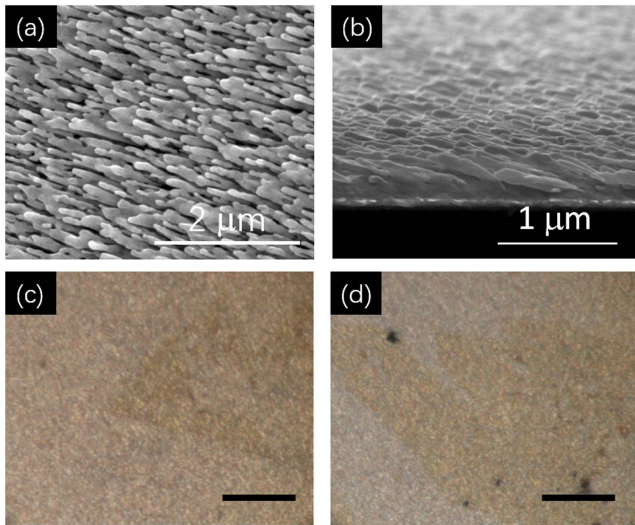


**Fig. 1.** (a) and (b) SEM (a) top-view and (b) tilted-view images of AgNR substrate. (c) and (d) Optical images of (c) MoS<sub>2</sub> and (d) MS<sub>2</sub> on AgNR substrate. The scale bars are 10 μm.

images of transferred MS<sub>2</sub> monolayers on AgNRs. Though the exposed AgNRs might be oxidized during the baking, the AgNRs covered by MS<sub>2</sub> monolayer were not oxidized. Because significant variations were already observed between samples on different dielectric substrates and with different film-substrate bonding conditions [2], and different annealing processes [23], a set of MS<sub>2</sub> samples with varying preparation conditions but all on dielectric substrates were included in this study for highlighting the more drastic differences between the AgNR substrate and dielectric substrates in general. Samples with suspended MS<sub>2</sub> monolayers were used as the reference.

Raman measurements were performed with a Horiba LabRAM HR800 Raman microscope using a 441.6 nm laser with a 100× objective lens (NA = 0.9). The plasmon absorption peak for the AgNRs is ~430 nm [24], which is close to the laser excitation line. An additional reason to use 441.6 nm excitation rather than more commonly used 532 nm is to avoid the resonant Raman effect of WS<sub>2</sub> monolayer whose B-exciton bandgap matches the energy of 532 nm excitation [2]. The spectral resolution is better than 1 cm<sup>-1</sup>. All Raman signals were acquired with a laser power of ~20 μW, sufficiently low to avoid potential sample heating and degradation.

Five MoS<sub>2</sub> samples were prepared on different substrates, including: (1) transferred on AgNR substrate (MoS<sub>2</sub>-Ag), (2) as-grown on a sapphire substrate (MoS<sub>2</sub>-SA), (3) transferred on a sapphire substrate (MoS<sub>2</sub>-Tran-SA), (4) transferred on a patterned SiO<sub>2</sub>/Si substrate with both supported region (MoS<sub>2</sub>-Tran-SiO<sub>2</sub>-supported) and suspended region over a hole (MoS<sub>2</sub>-Tran-SiO<sub>2</sub>-suspended), and (5) transferred on a SiO<sub>2</sub>/Si substrate without annealing (MoS<sub>2</sub>-Tran-SiO<sub>2</sub>-NA). Their optical images are shown in Fig. 1(c) and Figs. 2(a)–2(d). A Raman mapping on a continuous area of the as-grown MoS<sub>2</sub>-SA was performed to confirm the thickness of MoS<sub>2</sub> as monolayer. The spatial variation of the Raman shift difference ( $\Delta\nu$ ) between  $A_{1g}$  and  $E_{2g}$  modes is shown in Fig. 2(e). The values of  $\Delta\nu$  in the mapped area are less than 20 cm<sup>-1</sup>, indicating that the as-grown film is indeed monolayer [25]. Figure 2(f) shows six typical Raman spectra from above five samples

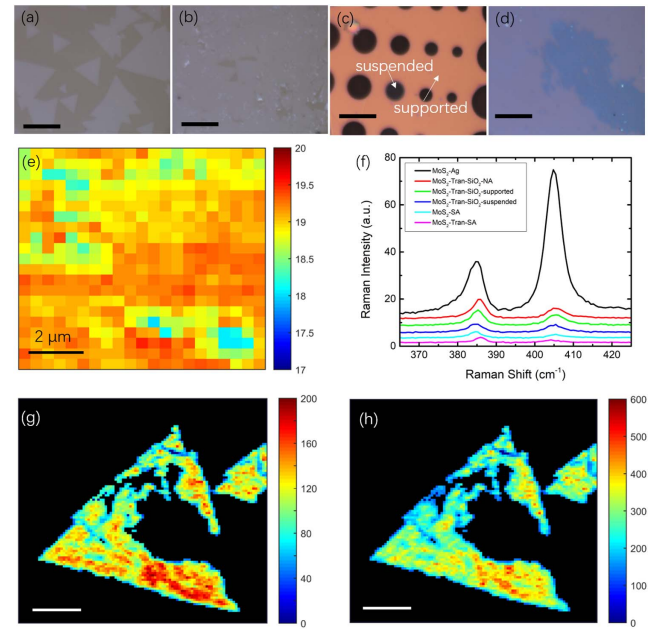


**Fig. 2.** Optical images of four MoS<sub>2</sub> samples: (a) MoS<sub>2</sub>-SA, (b) MoS<sub>2</sub>-Tran-SA, (c) MoS<sub>2</sub>-Tran-SiO<sub>2</sub>-supported and MoS<sub>2</sub>-Tran-SiO<sub>2</sub>-suspended on the same substrate, and (d) MoS<sub>2</sub>-Tran-SiO<sub>2</sub>-NA. The scale bars are 10 μm. (e) Map of frequency difference between  $A_{1g}$  and  $E_{2g}$  modes for MoS<sub>2</sub>-Ag. (f) Typical Raman spectra of all MoS<sub>2</sub> samples. (g) and (h) The integral intensity mappings of (g)  $E_{2g}$  and (h)  $A_{1g}$  modes. The scale bars are 10 μm.

(six supporting situations). Their  $E_{2g}$  and  $A_{1g}$  peak positions, intensities,  $\Delta\nu$ , and relative intensity of  $A_{1g}$  and  $E_{2g}$  modes,  $R = I(A_{1g})/I(E_{2g})$ , are summarized in Table 1. The peak intensities in Table 1 have been normalized to the  $E_{2g}$  intensity of MoS<sub>2</sub>-Tran-SiO<sub>2</sub>-suspended. The Raman shifts of two Raman modes,  $E_{2g}$  and  $A_{1g}$ , are ~385 and ~405 cm<sup>-1</sup>, respectively, for all samples. The small variations in Raman frequency for both modes have been attributed to the strain and the doping effects [26,27]. The discussion of the specific mechanisms is beyond the focus of this work. However, the values of  $\Delta\nu$  indicate that all the MoS<sub>2</sub> samples are monolayer. Some variations in intensity do exist between samples on different dielectric substrates, but to a much less extent compared to

**Table 1.**  $E_{2g}$  and  $A_{1g}$  Peak Positions, Intensities, Separation  $\Delta\nu$ , and Relative Intensity,  $R = I(A_{1g})/I(E_{2g})$ , of MoS<sub>2</sub> Samples

MoS <sub>2</sub> Samples	Raman Frequency (cm <sup>-1</sup> )			Raman Intensity		
	$\nu(E_{2g})$	$\nu(A_{1g})$	$\Delta\nu$	$I(E_{2g})$	$I(A_{1g})$	R
MoS <sub>2</sub> -SA	384.6	405.5	20.9	0.58	0.38	0.66
MoS <sub>2</sub> -Tran-SA	385.9	404.3	18.4	0.40	0.31	0.76
MoS <sub>2</sub> -Tran-SiO <sub>2</sub> -suspended	384.5	405.1	20.6	<b>1.00</b>	1.04	1.04
MoS <sub>2</sub> -Tran-SiO <sub>2</sub> -supported	385.1	405.6	20.5	1.56	1.57	1.01
MoS <sub>2</sub> -Tran-SiO <sub>2</sub> -NA	385.5	405.6	20.1	1.92	1.40	0.73
MoS <sub>2</sub> -Ag	384.4	405.0	20.6	6.76	18.54	2.74

the effects of the AgNR substrate. For instance, the Raman signals of the films on the SiO<sub>2</sub>/Si substrate, annealed or not, are somewhat stronger than those on the sapphire substrate. As already discussed in the literature, this is due to the enhancement originating from the optical interference effect within the heterostructure of SiO<sub>2</sub>/Si samples [1,28]. However, the enhancement of both Raman modes on the MoS<sub>2</sub>-Ag sample is much more drastic. Compared to MoS<sub>2</sub>-Tran-SiO<sub>2</sub>-suspended, the integrated Raman intensities of  $E_{2g}$  and  $A_{1g}$  modes are enhanced by 6.8 and 17.7, respectively, which is attributed to the plasmonic enhancement of the AgNR substrate.

The  $R$  values given are typical values extracted from the Raman spectra of Fig. 2(f). The ratio  $R$  is significantly enhanced, changed from  $R = 1.04$  for MoS<sub>2</sub>-Tran-SiO<sub>2</sub>-suspended to  $R = 2.74$  for MoS<sub>2</sub>-Ag. The moderate variations in the ratio  $R$ 's of the samples on dielectric substrates are typically attributed to the doping effect that is known to affect  $A_{1g}$  more than  $E_{2g}$ . The spatial variations of the  $E_{2g}$  and  $A_{1g}$  intensities of the MoS<sub>2</sub>-Ag sample are shown in Figs. 2(g) and 2(h), respectively. It is significant to note that the Raman enhancement occurs over areas up to 10 to 20  $\mu\text{m}$  in size in this nonoptimized attempt. Overall, the Raman signal intensities of MoS<sub>2</sub>-Ag are enhanced by a factor of 2–8 and 5–20 times for  $E_{2g}$  and  $A_{1g}$ , respectively, relative to those of MoS<sub>2</sub>-Tran-SiO<sub>2</sub>-suspended. In contrast to the approach of adding metallic particles on top of the 2D layer, this approach can potentially offer much more uniform enhancement over a large area of a 2D layer. Further improvement in uniformity can be expected through improving both the Ag substrate uniformity and the transfer practice.

A similar set of four WS<sub>2</sub> samples were studied, including: (1) transferred on a AgNR substrate (WS<sub>2</sub>-Ag), (2) as-grown on a sapphire substrate (WS<sub>2</sub>-SA), (3) transferred on a patterned SiO<sub>2</sub>/Si substrate with both supported region (WS<sub>2</sub>-Tran-SiO<sub>2</sub>-supported) and suspended region (WS<sub>2</sub>-Tran-SiO<sub>2</sub>-suspended), and (4) transferred on a SiO<sub>2</sub>/Si substrate without annealing (WS<sub>2</sub>-Tran-SiO<sub>2</sub>-NA). Their optical images are shown in Fig. 1(d) and Figs. 3(a)–3(c). Raman mapping of the as-grown WS<sub>2</sub>-SA sample yielded the distribution of frequency difference  $\Delta\nu$  between  $A_{1g}$  and  $E_{2g}$  shown in Fig. 3(d). The difference is mostly less than 62  $\text{cm}^{-1}$ , indicating the as-grown WS<sub>2</sub> film is largely monolayer [29]. Figure 3(e) compares the typical Raman spectra from the four samples. Their  $E_{2g}$  and  $A_{1g}$  peak positions, intensities,  $\Delta\nu$ , and relative intensity ratios  $R$  are summarized in Table 2. The peak intensities in Table 2 have been normalized to the  $E_{2g}$  intensity of WS<sub>2</sub>-Tran-SiO<sub>2</sub>-suspended. The results of WS<sub>2</sub> are qualitatively similar to MoS<sub>2</sub>. Again, the variations between the samples on dielectric substrates are substantially smaller than the changes induced by the AgNR substrate. The  $R$  value increases from 0.35 for WS<sub>2</sub>-Tran-SiO<sub>2</sub>-suspended to 0.96 for WS<sub>2</sub>-Ag. As the intensity maps of  $E_{2g}$  and  $A_{1g}$  show in Figs. 3(f) and 3(g), the enhancement clearly occurs at all places of the 2D film. Compared to the suspended WS<sub>2</sub> sample, the intensity enhancement factor of the  $E_{2g}$  mode is 2–5, and that of the  $A_{1g}$  mode is 8–23, respectively, for WS<sub>2</sub>-Ag. Compared to MoS<sub>2</sub>-Ag, the absolute enhancement factors in WS<sub>2</sub> are statistically at the same range for the individual peaks, but the relative enhancement ratio  $R$  is somewhat less.

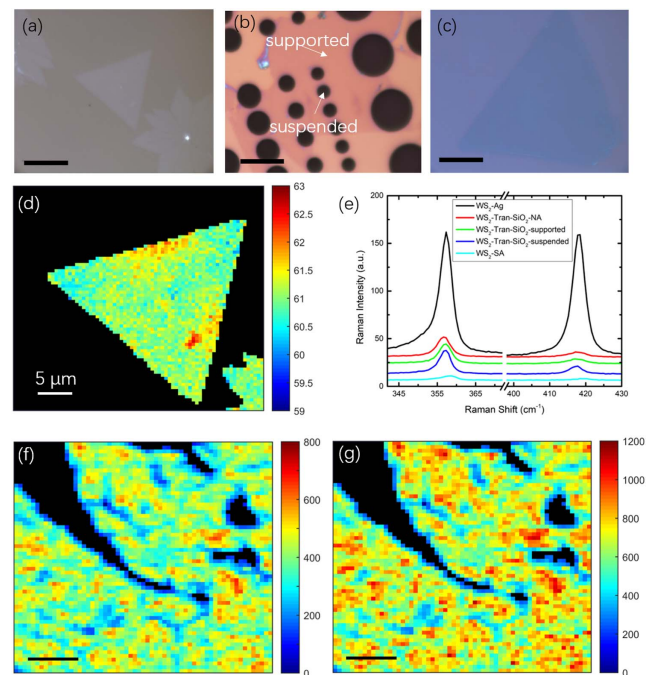


**Fig. 3.** Optical images of three WS<sub>2</sub> samples: (a) WS<sub>2</sub>-SA, (b) WS<sub>2</sub>-Tran-SiO<sub>2</sub>-supported and WS<sub>2</sub>-Tran-SiO<sub>2</sub>-suspended on the same substrate, and (c) WS<sub>2</sub>-Tran-SiO<sub>2</sub>-NA. The scale bars are 10  $\mu\text{m}$ . (d) Map of frequency difference between  $A_{1g}$  and  $E_{2g}$  modes for WS<sub>2</sub>-Ag. (e) Typical Raman spectra of all WS<sub>2</sub> samples. (f) and (g) The integral intensity mappings of (f)  $E_{2g}$  and (g)  $A_{1g}$  modes. The scale bar is 5  $\mu\text{m}$ .

Figures 4(a) and 4(b) show the distributions of the measured relative enhancement,  $r = R(\text{AgNR})/R(\text{suspended})$ , over the mapped areas for both MoS<sub>2</sub> and WS<sub>2</sub> on the AgNR substrate. Despite some variations, the  $r$  values are consistently greater than 1 for both MoS<sub>2</sub> and WS<sub>2</sub> films, indicating that the enhancement to the  $A_{1g}$  mode is greater than that to the  $E_{2g}$  mode. This trend can be explained below. Each AgNR can be viewed as a metallic tip similar to that used in tip-enhanced Raman scattering (TERS), as shown schematically in Fig. 4(c). When excited under p-polarization, the highest local electric field is found near the tip of the nanorod [30], which explains the overall effectiveness of the enhancement to both modes. Each AgNR could be viewed as a radiating dipole with the direction of the field along the axis direction at the tip. The field

**Table 2.**  $E_{2g}$  and  $A_{1g}$  Peak Positions, Intensities,  $\Delta\nu$ , and  $R$  Values of WS<sub>2</sub> Samples

WS <sub>2</sub> Samples	Raman Frequency ( $\text{cm}^{-1}$ )			Raman Intensity		
	$\nu(E_{2g})$	$\nu(A_{1g})$	$\Delta\nu$	$I(E_{2g})$	$I(A_{1g})$	$R$
WS <sub>2</sub> -SA	357.9	419.1	61.2	0.24	0.08	0.34
WS <sub>2</sub> -Tran-SiO <sub>2</sub> -suspended	357.0	417.3	60.3	<b>1.00</b>	0.35	0.35
WS <sub>2</sub> -Tran-SiO <sub>2</sub> -supported	357.0	417.4	60.4	0.89	0.31	0.34
WS <sub>2</sub> -Tran-SiO <sub>2</sub> -NA	356.6	417.6	61	0.96	0.31	0.32
WS <sub>2</sub> -Ag	357.2	418.0	60.8	5.85	5.63	0.96

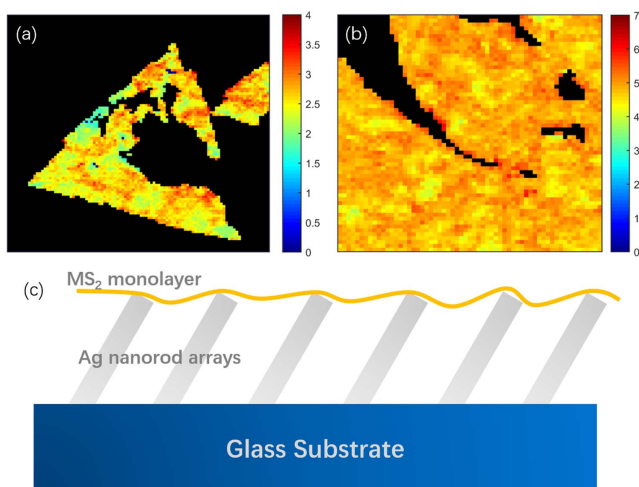


**Fig. 4.** (a) and (b) Maps of the intensity ratio of  $A_{1g}$  over  $E_{2g}$  for (a) MoS<sub>2</sub>-Ag and (b) WS<sub>2</sub>-Ag. (c) Schematic diagram of MS<sub>2</sub> monolayer on AgNR substrate.

is more localized along the vertical than lateral direction of the 2D film, thus favoring  $A_{1g}$  over  $E_{2g}$ . The magnitudes and ratio  $R$  are expected to depend on the inclined angle of AgNRs and laser polarization and incidence angle. The difference could also be related to charge transfer between the nanorod and film. It is known that the  $A_{1g}$  phonon is more sensitive to doping [26], which means it has a stronger coupling with electrons. The charge exchange between the AgNR substrate and MS<sub>2</sub> film likely occurs, so the enhancement effect could also be affected by the charge transfer. However, the doping effect tends to affect more the  $A_{1g}$  peak position than the intensity, at least not to the extent comparable to what has been observed in this study. Therefore, we suggest the primary mechanism for the enhancement is the electromagnetic or plasmonic effect.

The enhancement effects are statistically similar between WS<sub>2</sub> and MoS<sub>2</sub> under 441.6 nm excitation. The spatial fluctuations in intensity for both modes shown in Figs. 2(g) and 2(h), and Figs. 3(f) and 3(g), and the  $r$  values in Fig. 4 could be understood as the variation in the contact between the AgNR and the film [as illustrated in Fig. 4(c)] and the tip condition, which could be optimized.

In summary, compared to MS<sub>2</sub> layers on dielectric substrates, the SERS study of MS<sub>2</sub> monolayers on the AgNR substrate has been shown to offer more dramatic enhancement on the Raman intensity for both  $E_{2g}$  and  $A_{1g}$  Raman modes. The enhancement is primarily attributed to the electromagnetic or plasmonic effect. We have also found that the intensity ratio of  $A_{1g}$  over  $E_{2g}$  is much greater for MS<sub>2</sub>-Ag samples than that on other substrates investigated in this work, indicating a stronger enhancement for the  $A_{1g}$  mode than the  $E_{2g}$  mode. However, the overall and relative enhancements to the two modes are expected to be tunable by varying the design of the AgNR substrate. Optimization could lead to a more uniform and stronger enhancement effect. This work, on one hand, can benefit the fundamental study of the 2D-TMDs and facilitate the applications that rely on the strength of the optical signal of the 2D layer, and, on the other hand, provide the foundation to develop 2D-TMD SERS substrates for probing chemical molecules.

**Funding.** National Science Foundation (ECCS-1611330); Army Research Office (W911NF-13-1-0201).

**Acknowledgment.** Y. Z. acknowledges the support of the Bissell Distinguished Professorship.

## REFERENCES

1. N. Scheuschner, O. Ochedowski, A.-M. Kaulitz, R. Gillen, M. Schleberger, and J. Maultzsch, *Phys. Rev. B* **89**, 125406 (2014).
2. L. Su, Y. Yu, L. Cao, and Y. Zhang, *Nano Res.* **8**, 2686 (2015).
3. Y. Yu, Y. Yu, C. Xu, Y.-Q. Cai, L. Su, Y. Zhang, Y.-W. Zhang, K. Gundogdu, and L. Cao, *Adv. Funct. Mater.* **26**, 4733 (2016).
4. L. Britnell, R. M. Ribeiro, A. Eckmann, R. Jalil, B. D. Belle, A. Mishchenko, Y. J. Kim, R. V. Gorbachev, T. Georgiou, S. V. Morozov, A. N. Grigorenko, A. K. Geim, C. Casiraghi, A. H. C. Neto, and K. S. Novoselov, *Science* **340**, 1311 (2013).
5. J. Lin, H. Li, H. Zhang, and W. Chen, *Appl. Phys. Lett.* **102**, 203109 (2013).
6. X. Yang, W. Liu, M. Xiong, Y. Zhang, T. Liang, J. Yang, M. Xu, J. Ye, and H. Chen, *J. Mater. Chem. A* **2**, 14798 (2014).
7. S. S. Singha, D. Nandi, and A. Singha, *RSC Adv.* **5**, 24188 (2015).
8. Y. Deng, M. Chen, J. Zhang, Z. Wang, W. Huang, Y. Zhao, J. P. Nshimiyimana, X. Hu, X. Chi, G. Hou, X. Zhang, Y. Guo, and L. Sun, *Nano Res.* **9**, 1682 (2016).
9. D. Jariwala, A. R. Davoyan, J. Wong, and H. A. Atwater, *ACS Photon.* **4**, 2962 (2017).
10. J. Lu, J. H. Lu, H. Liu, B. Liu, L. Gong, E. S. Tok, K. P. Loh, and C. H. Sow, *Small* **11**, 1792 (2015).
11. J. Ping, Z. Fan, M. Sindoro, Y. Ying, and H. Zhang, *Adv. Funct. Mater.* **27**, 1605817 (2017).
12. S. Su, C. Zhang, L. Yuwen, J. Chao, X. Zuo, X. Liu, C. Song, C. Fan, and L. Wang, *ACS Appl. Mater. Interface* **6**, 18735 (2014).
13. J. Zhao, Z. Zhang, S. Yang, H. Zheng, and Y. Li, *J. Alloys Compd.* **559**, 87 (2013).
14. J. Xu, C. Li, H. Si, X. Zhao, L. Wang, S. Jiang, D. Wei, J. Yu, X. Xiu, and C. Zhang, *Opt. Express* **26**, 21546 (2018).
15. C. Zhang, C. Li, J. Yu, S. Jiang, S. Xu, C. Yang, Y. J. Liu, X. Gao, A. Liu, and B. Man, *Sens. Actuators B Chem.* **258**, 163 (2018).
16. Y. Shi, J.-K. Huang, L. Jin, Y.-T. Hsu, S. F. Yu, L.-J. Li, and H. Y. Yang, *Sci. Rep.* **3**, 1839 (2013).
17. J.-C. Dong, X.-G. Zhang, V. Briega-Martos, X. Jin, J. Yang, S. Chen, Z.-L. Yang, D.-Y. Wu, J. M. Feliu, C. T. Williams, Z.-Q. Tian, and J.-F. Li, *Nat. Energy* **4**, 60 (2019).
18. E. L. Ru and P. Etchegoin, *Principles of Surface-Enhanced Raman Spectroscopy and Related Plasmonic Effects* (Elsevier, 2008).
19. S. B. Chaney, S. Shanmukh, R. A. Dluhy, and Y.-P. Zhao, *Appl. Phys. Lett.* **87**, 031908 (2005).
20. J. D. Driskell, S. Shanmukh, Y. Liu, S. B. Chaney, X. J. Tang, Y. P. Zhao, and R. A. Dluhy, *J. Phys. Chem. C* **112**, 895 (2008).
21. Y. Yu, C. Li, Y. Liu, L. Su, Y. Zhang, and L. Cao, *Sci. Rep.* **3**, 1866 (2013).
22. A. Gurarslan, Y. Yu, L. Su, Y. Yu, F. Suarez, S. Yao, Y. Zhu, M. Ozturk, Y. Zhang, and L. Cao, *ACS Nano* **8**, 11522 (2014).
23. W. Su, N. Kumar, A. Krayev, and M. Chaigneau, *Nat. Commun.* **9**, 2891 (2018).
24. Y.-P. Zhao, S. B. Chaney, and Z.-Y. Zhang, *J. Appl. Phys.* **100**, 063527 (2006).
25. H. Li, Q. Zhang, C. C. R. Yap, B. K. Tay, T. H. T. Edwin, A. Olivier, and D. Baillargeat, *Adv. Funct. Mater.* **22**, 1385 (2012).
26. B. Chakraborty, A. Bera, D. V. S. Muthu, S. Showmick, U. V. Waghmare, and A. K. Sood, *Phys. Rev. B* **85**, 161403 (2012).
27. C. Rice, R. J. Young, R. Zan, U. Bangert, D. Wolverson, T. Georgiou, R. Jalil, and K. S. Novoselov, *Phys. Rev. B* **87**, 081307 (2013).
28. M. Buscema, G. A. Steele, H. S. J. van der Zant, and A. Castellanos-Gomez, *Nano Res.* **7**, 561 (2014).
29. A. Berkdemir, H. R. Gutiérrez, A. R. Botello-Méndez, N. Perea-López, A. L. Elías, C.-I. Chia, B. Wang, V. H. Crespi, F. López-Urías, J.-C. Charlier, H. Terrones, and M. Terrones, *Sci. Rep.* **3**, 1755 (2013).
30. Y. J. Liu, Z. Y. Zhang, Q. Zhao, R. A. Dluhy, and Y. P. Zhao, *J. Phys. Chem. C* **113**, 9664 (2009).